

1

2 **Accepted Author Manuscript (AAM)**

3

---

4

5 **Article Title:** Electrochemical degradation of tebuthiuron pesticide using

6 a flow reactor: Insights into co-generation of oxidants and

7 ecotoxicological risks

8

9

10 **Authors:** Robson S. Souto, Isaac Sánchez-Montes, Géssica O.S. Santos, Paulo J. M.

11 Cordeiro-Junior, Renata Colombo, Mauro C. Santos, Marcos R. V. Lanza

12

13

14

15

16 DOI: <http://dx.doi.org/10.1016/j.jece.2025.115528>

17

18 Journal: *Journal of Environmental Chemical Engineering*

19 Received date: 31 August 2024

20 Revised date: 28 October 2024

21 Accepted date: 18 January 2025

22

23

24

25

---

26 Copyright Notice:

27

28 This is the accepted version of the following article: Robson S. Souto, Isaac

29 Sánchez-Montes, Géssica O.S. Santos, Paulo J. M. Cordeiro-Junior, Renata Colombo,

30 Mauro C. Santos, Marcos R. V. Lanza, Electrochemical degradation of tebuthiuron

31 pesticide using a flow reactor: Insights into co-generation of oxidants and

32 ecotoxicological risks, *Journal of Environmental Chemical Engineering*, (2025),

33 doi:<http://dx.doi.org/10.1016/j.jece.2025.115528>.

34

35

36 This manuscript version is made available under Elsevier's sharing policy and may be

37 shared in institutional repositories and non-commercial platforms after an embargo

38 period of 24 months from the publication date.

39

40 © 2025 Elsevier. This manuscript is for non-commercial purposes only and must not

41 be modified or enhanced by third parties.

42

43

44      **Electrochemical degradation of tebuthiuron pesticide**  
45      **using a flow reactor: Insights into the co-generation of**  
46      **oxidants and ecotoxicological risks**

47

48

49      Robson S. Souto<sup>1,2\*</sup>, Isaac Sánchez-Montes<sup>1</sup>, Géssica O. S. Santos<sup>1</sup>, Paulo J. M.  
50      Cordeiro-Junior<sup>1</sup>, Renata Colombo<sup>2</sup>, Mauro C. Santos<sup>3</sup>, Marcos R. V. Lanza<sup>1,\*</sup>

51

52

53

54      <sup>1</sup>*São Carlos Institute of Chemistry, University of São Paulo, 13560-970, São Carlos, SP, Brazil*

55      <sup>2</sup>*School of Arts, Sciences and Humanities, University of São Paulo, 03828-000, São Paulo, SP,  
56      Brazil*

57      <sup>3</sup>*Center of Natural and Human Sciences, Federal University of ABC. Rua Santa Adélia 166,  
58      Bairro Bangu, 09210-170, Santo André, SP, Brazil*

59      <sup>4</sup>*University of State of Mato Grosso, 78200-000, Av. Tancredo Neves - Cavalhada III, Cáceres,  
60      MT, Brazil.*

61

62

63      \*Corresponding author:

64      Robson S. Souto ([robsonssouto@gmail.com](mailto:robsonssouto@gmail.com))

65      Marcos R. V. Lanza (marcoslanza@usp.br)

66

67

68

69

70

71

72

73

74

## ABSTRACT

Innovative contaminants treatment approaches are essential to addressing persistent environmental contamination from pesticides such as tebuthiuron (TBT), as they provide us with more effective and safer alternatives to traditional degradation methods. A notable advanced treatment approach is the combined electrochemical process which involves ultraviolet-C (UVC) activation of *in-situ* electrogenerated H<sub>2</sub>O<sub>2</sub> and chlorine species – the combined UVC/e-H<sub>2</sub>O<sub>2</sub>@e-ClO<sup>-</sup> system. This method uses an electrochemical flow reactor equipped with a gas diffusion cathode and a DSA®-Cl<sub>2</sub> anode, allowing the simultaneous production of both oxidants. Under the best experimental conditions (10 mA cm<sup>-2</sup>, 10 mmol L<sup>-1</sup> of Cl<sup>-</sup>, and pH 7), the combined UVC/e-H<sub>2</sub>O<sub>2</sub>@e-ClO<sup>-</sup> system promoted over 99.0% TBT degradation in 60 min of treatment and 63.2% total organic carbon removal in 90 min, with low energy consumption (1.54 kWh g<sup>-1</sup> TOC). The roles of different reactive oxygen species (H<sub>2</sub>O<sub>2</sub>, HClO/ClO<sup>-</sup>, and hydroxyl radicals (HO<sup>•</sup>)) were also evaluated, and a mineralization pathway was proposed based on the analysis of the by-products generated under the different electrochemical conditions. Although several by-products were detected during the degradation process, toxicological estimations suggested that these intermediates are less toxic than the parent compound; in this sense, it is evident that the degradation process helps reduce the environmental impact of TBT. Thus, the combined electrochemical process of activating H<sub>2</sub>O<sub>2</sub> and chlorine species effectively degrades organic pollutants in chloride-containing wastewater, offering a sustainable and efficient treatment solution. Additionally, while TBT degradation has been extensively studied in the literature, it is the first time that a combined UVC/e-H<sub>2</sub>O<sub>2</sub>@e-ClO<sup>-</sup> approach has been employed to investigate this contaminant and its toxicity effects following treatment.

100

101 **Keywords:** electrochemical flow reactor, gas diffusion cathode, in-situ hydrogen  
102 peroxide, reactive chlorine species, tebuthiuron degradation, toxicological assessment.

103

104

105 **1 Introduction**

106        Electrochemical advanced oxidation processes (EAOP) are considered a highly  
107    promising technique for water treatment due to their adaptability and on-demand  
108    operability. Unlike traditional methods, EAOPs can be used to treat matrices with  
109    varying contaminant levels; for instance, the treatment of industrial wastewater  
110   (effluent) often requires more treatment steps due to its higher contaminant  
111   concentration levels compared to raw water intended for human consumption. In view  
112   of that, EAOPs have been found to be extremely more efficient when applied for the  
113   treatment of industrial wastewater with high contaminant concentration levels and  
114   fluctuating water quality compared to raw water [1]. Furthermore, the decentralized  
115   nature of the EAOP treatment mechanism enables its deployment in diverse settings,  
116   from urban centers to remote communities [2]. However, most studies involving the use  
117   of EAOPs have focused their attention on the application of small-scale laboratory cells  
118   for wastewater remediation [3]. The present work aims to bridge this gap by using an  
119   electrochemical flow reactor (EFR) with higher flow rates to treat contaminants of high  
120   concentration in large-scale applications.

121        To add to the advantages of the EAOP technology, some studies have combined  
122   the process involving the electrogeneration of oxidants at the anode or cathode with UV  
123   irradiation or Fenton reaction to generate more reactive species [4]; however, these  
124   studies have typically been confined to a single electrode for either direct degradation or  
125   oxidant generation. To enhance the efficiency of EAOP systems, some studies have  
126   explored the co-electrogeneration of oxidants simultaneously at the anode and cathode,  
127   and often in combination with UV irradiation or Fenton reaction; one major  
128   shortcoming of these studies lies in their use of separate compartments with ion  
129   exchange membranes (IEM) to isolate and analyze the effects of each electrode process

130 [5–7]. As noted previously, the interaction of different oxidants within the same  
131 chamber can undermine the degradation efficiency [8,9]. Unfortunately, using IEM  
132 increases the costs of the electrochemical treatment system, and makes its maintenance  
133 quite difficult. To address these challenges, we propose the use of a membrane-less  
134 electrochemical system for the in-situ co-generation of oxidants for wastewater  
135 remediation purposes. To the best of our knowledge, no work reported in the literature  
136 has employed this approach to date.

137 The formation of toxic by-products in water treatment processes is a matter of  
138 huge concern, especially when the processes involve chlorine-based oxidants [10].  
139 While these chlorine-based processes remove contaminants, they can also generate toxic  
140 by-products [11]. As pointed out in the literature, while chlorination can increase the  
141 toxicity of the treated solution, combining this treatment mechanism with UV light can  
142 help reduce the toxicity level [12,13]. Treatment systems that combine  $\text{H}_2\text{O}_2$  with UVC  
143 often yield fewer toxic by-products. Oddly enough, there is an alarming scarcity of  
144 studies that have investigated the toxicity nature of the by-products formed during TBT  
145 degradation based on the combined application of electrogenerated  $\text{H}_2\text{O}_2$  and  
146 hypochlorite ( $\text{ClO}^-$ ) with UVC.

147 Tebuthiuron (TBT) is a widely popular herbicide which is commonly used for  
148 weed control mainly in sugar cane cultivations in Brazil; the compound is known for its  
149 very high persistence in the environment [14]. Because of its extremely high solubility  
150 in water ( $2.3 \text{ g L}^{-1}$  at  $25^\circ\text{C}$ ), this pesticide is frequently detected in both surface water  
151 and groundwater [14]. TBT is regarded as highly toxic by the Brazilian Health  
152 Surveillance Agency in Brazil (ANVISA) [15]. Due to its characteristics, TBT was  
153 selected as model pollutant for the conduct of degradation analysis in the present study.  
154 A number of studies reported in the literature have investigated TBT degradation using

155 a wide range of alternative treatment technologies including electrochemical oxidation  
156 with dimensional stable anodes [16], boron doped diamond anodes [17], UVC-based  
157 technologies [18], and solar photo-Fenton [19]. In particular, the use of chlorine as  
158 precursor of reactive oxygen and chlorine radicals in the aforementioned TBT  
159 degradation techniques has been found to present some underlying disadvantages; these  
160 include the possible formation of organochlorine compounds and concerns regarding  
161 environmental safety with respect to the use of chlorine. Among the main advantages of  
162 the in-situ co-generation of oxidants such as  $H_2O_2$  and  $ClO^-$  and its activation using  
163 UVC include the following: i) lack of the need for oxidants transportation, and ii) highly  
164 efficient and fast contaminants degradation rates. It is worth highlighting that the central  
165 idea of our proposed treatment approach lies in using a Printex® L6 carbon gas diffusion  
166 electrode, which is well known for its high selectivity for  $H_2O_2$  generation, and a  
167 commercial DSA® anode, which is widely recognized for its ability to generate chlorine  
168 species. In essence, by employing these electrodes in the treatment system, the approach  
169 is expected to promote high degradation efficiency from the successful combination of  
170 the electrogenerated oxidants. The identification of by-products formed during TBT  
171 degradation and the analysis of their toxicity are found to be of great importance.  
172 Indeed, among the main novel contributions of the present study is the use of suitable  
173 tools to estimate acute and chronic toxicity in TBT degradation for the first time under  
174 the proposed treatment system.

175 In short, the present study employs for the first time an electrochemical flow  
176 reactor in a recirculation system for the *in-situ* electrogeneration of  $H_2O_2$  and  $ClO^-$   
177 oxidants targeted at the degradation of TBT herbicide. Different treatment systems -  
178 including photolysis (UVC), anodic oxidation (AO), electrogenerated  $H_2O_2$  and  $ClO^-$   
179 oxidants ( $e-H_2O_2$  and  $e-ClO^-$ ), and their combinations were evaluated. The study also

180 investigated the role of the electrogenerated oxidants and radical species ( $\text{ClO}^\bullet$ ,  $\text{Cl}^\bullet$  and  
181  $\text{HO}^\bullet$ ) in TBT mineralization, and pathways for TBT degradation were proposed. In  
182 addition, we also conducted a toxicological analysis of the by-products formed using a  
183 Quantitative Structure-Activity Relationship (QSAR) model.

184

## 185 2 Materials and Methods

### 186 2.1 *Chemicals*

187 The following compounds were used for the preparation of the electrolyte and  
188 for pH control: potassium sulfate ( $\text{K}_2\text{SO}_4$ ), sodium chloride ( $\text{NaCl}$ ), sulfuric acid  
189 ( $\text{H}_2\text{SO}_4$ ), and potassium hydroxide ( $\text{KOH}$ ) - all chemicals were of 99.9% purity.  $\text{H}_2\text{O}_2$   
190 was quantified using the complexing  $0.5 \text{ mol L}^{-1}$   $\text{H}_2\text{SO}_4$  solution containing ammonium  
191 molybdate ( $(\text{NH}_4)_6\text{Mo}_7\text{O}_{24}$ ). For the preparation of the electrode, we employed a  
192 commercial Printex L6 carbon (PL6C) (purchased from Evonik) mixture with  
193 poly(tetrafluoroethylene) (PTFE, 60% aqueous dispersion) - obtained from Daklon 1  
194 (Sealflon). For the construction of the calibration curves using the analytical procedure,  
195 we employed standard tebuthiuron (purchased from Sigma-Aldrich). For the  
196 degradation process, we prepared a solution concentration of  $100 \text{ }\mu\text{mol L}^{-1}$  of the  
197 pesticide tebuthiuron with 50% w/V (commercial grade) - acquired from Dow  
198 AgroScience (Combine 500 SC). All solutions were prepared using ultrapure water,  
199 obtained from the Milli-Q system (resistivity  $>18 \text{ M}\Omega \text{ cm}$ ).

### 200 2.2 *Preparation of Gas Diffusion Electrode (GDE)*

201 The gas diffusion electrode (GDE) was prepared based on the method previously  
202 described by our research group [20]. Briefly, the gas diffusion layer was prepared by

203 mixing PL6C with PTFE. The mixture containing PL6C and PTFE was prepared in the  
204 ratio of 80 (PL6C) to 20 (PTFE) (w/w). The mixture was spread on a thin layer over  
205 carbon cloth - obtained from ZOLTEK. Finally, the mixture/cloth was hot pressed by  
206 applying 4.5 tons at 290 °C for 15 min.

207 *2.3 Electrochemical Flow Reactor Setup*

208 The electrochemical flow reactor (EFR) used in this work has already been  
209 characterized and reported in a previous work published in the literature [21]; the EFR  
210 design is presented in Fig. 1. The GDE, used as cathode, is sequentially connected to a  
211 stainless-steel mesh (current collector) and a gas chamber filled with O<sub>2</sub>. A  
212 dimensionally stable anode with chlorine (DSA®-Cl<sub>2</sub>) (from De Nora do Brasil) was  
213 used as anode. Both electrodes (GDE cathode and DSA®-Cl<sub>2</sub> anode) had an exposed  
214 geometric area of 20 cm<sup>2</sup>.

215

216 **Fig. 1. a)** EFR configuration; **b)** internal design of the flow reactor with gap between  
217 the electrodes.

218 The system setup used for TBT degradation is presented in Fig. 2. A semi-batch  
219 configuration was used; the system consisted of a reservoir tank (with 1.0 L solution),  
220 where the temperature (~22.0 °C) is controlled using a thermostatic bath. A power  
221 source controlling the current passing through the EFR is fed by a peristaltic pump  
222 operating at the flow rate of 30 L h<sup>-1</sup>. Behind the outlet of the EFR, a chamber  
223 containing a low-pressure Hg lamp (254 nm; Philips 9W) is used to activate the  
224 electrogenerated oxidants. The gas flow rate is controlled by a flow meter and fed by an  
225 O<sub>2</sub> (99.9% purity) cylinder.

226

227 **Fig. 2.** Electrochemical Setup: **1)** Electrochemical flow reactor; **2)** UVC chamber; **3)**  
228 Reservoir tank; **4)** Peristaltic pump; **5)** Power source; **6)** Gas flow meter; **7)** Oxygen  
229 cylinder.

230 The electrogenerated  $\text{H}_2\text{O}_2$  was quantified by an indirect method using a  
231 complexant of ammonium molybdate ( $(\text{NH}_4)_6\text{Mo}_7\text{O}_{24}$ ) solution at  $2.4 \times 10^{-3} \text{ mol L}^{-1}$  [10].  
232 The complex formed (peroxymolybdate) was very stable, with absorbance measured at  
233 the wavelength of 350 nm. The analysis was performed using a UV-1900  
234 spectrophotometer (Shimadzu) and a quartz cuvette with 1 cm path length.

235 The power source was connected to two multi-meters (one in parallel and the  
236 other one in series) in order to guarantee the accuracy of the current and potential  
237 (measured). As reported, the EFR employed in this work has been previously studied  
238 and its current range efficiency has already been determined [21]. Taking these  
239 observations into account, the applied current range that would ensure the presence of  
240 enough  $\text{H}_2\text{O}_2$  for TBT degradation was set at 0.1 to 0.3 A (or  $5 - 15 \text{ mA cm}^{-2}$ ).  
241 Although the conductivity of wastewater is observed at  $15 \text{ mS cm}^2$ , we employed the  
242 ionic strength of  $0.3 \text{ mol L}^{-1}$  as control. In the tests involving the use of NaCl as a  
243 source of  $\text{Cl}^-$  ions, conductivity was adjusted, maintaining the same ionic strength.

244 *2.4 Analytical Procedures*

245 The degradation of TBT, salicylic acid (Sac. Ac.), 2,3 and 2,5 dihydroxybenzoic  
246 acid (2,3 and 2,5 DHBA) was analyzed by high-performance liquid chromatography  
247 (HPLC) using Shimadzu 20A LC system with a UV detector. A reversed-phase C18  
248 column was used as the stationary phase (150 mm  $\times$  4.6 mm, 5  $\mu\text{m}$  particle size, from

249 Phenomenex). All the analytical methods were first validated by calibration curves  
250 constructed using standard TBT; this was done in order to determine the concentration  
251 range, limit of detection (LOD), limit of quantification (LOQ), and linearity. All the  
252 samples collected were filtered using a 0.45  $\mu$ m Chromafil®Xtra PET filter (Macherey-  
253 Nagel) before analysis, and recovery tests were conducted with and without sample  
254 filtration.

255 For the analysis of only TBT degradation, we used a mobile phase which  
256 consisted of a mixture of 70% acetonitrile and 30% ultrapure water at a flow rate of 1  
257 mL min<sup>-1</sup>; elution was done in the isocratic mode. The standard range for the calibration  
258 curve was 0.31 - 20 mg L<sup>-1</sup>, with linearity of  $R^2=0.9993$  as the correlation. The limit of  
259 detection (LOD) and limit of quantification (LOQ) were  $1.56 \times 10^{-2}$  mg L<sup>-1</sup> and  $4.7 \times$   
260  $10^{-2}$  mg L<sup>-1</sup>. The recovery percentage obtained was 99.9%, with and without filtration.  
261 For Sac. Ac., 2,3 and 2,5 DHBA, a gradient elution method with a mixture of 50%  
262 acetonitrile and 50% aqueous solution of formic acid (0.1%) was employed. The sample  
263 injection employed was 20  $\mu$ L and the wavelength monitoring for TBT, Sac. Ac., 2,3  
264 and 2,5 DHBA was performed at 254, 300, 315 and 335 nm, respectively. The standard  
265 concentration range for the calibration curve was 3.1 - 125 mg L<sup>-1</sup> for the three  
266 compounds, with linearity of  $R^2=0.995$  as the correlation. The LOD recorded for Sac.  
267 Ac., 2,3 and 2,5 DHBA was  $3.4 \times 10^{-2}$ ,  $1.0 \times 10^{-2}$  and  $1.7 \times 10^{-2}$  mg L<sup>-1</sup>, respectively, while  
268 the LOQ recorded for Sac. Ac., 2,3 and 2,5 DHBA was 0.1,  $5.3 \times 10^{-2}$  and  $3.3 \text{ mgL}^{-1}$ ,  
269 respectively. For all the three compounds investigated, the recovery percentage obtained  
270 was 98.5%, with and without filtration.

271 The anions (NO<sub>3</sub><sup>-</sup>) were monitored by ion chromatography using Metrohm 850  
272 PRO IC coupled to Vario 940IC Extension Module with a conductivity detector. The  
273 MetrosepA Supp 5 column (150 mm/4.0 mm) was used as stationary phase for the

274 anionic species at 25 °C. The mobile phase, which was employed at a flow rate of 0.7  
275 mL min<sup>-1</sup>, consisted of Na<sub>2</sub>CO<sub>3</sub> and NaHCO<sub>3</sub> (3.2 and 1.0 mmol L<sup>-1</sup>, respectively). The  
276 standard concentration range for the calibration curve was 0.5 - 16 mg L<sup>-1</sup>, with linearity  
277 of R<sup>2</sup>=0.991 as the correlation. The LOD and LOQ recorded were 0.3 mg L<sup>-1</sup> and 1.1  
278 mg L<sup>-1</sup>, respectively. The recovery percentage obtained was 92%, with and without  
279 filtration. The rate of mineralization was evaluated through the analysis of total organic  
280 carbon (TOC) using Shimadzu TOC-VCPN. The standard concentration range for the  
281 calibration curve was 1.0 - 50 mg L<sup>-1</sup>, with linearity of R<sup>2</sup>=0.991 as the correlation.

282 The intermediates formed during the TBT degradation process were also  
283 determined by liquid chromatography tandem mass spectrometry (LC-MS/MS).  
284 However, for the separation and detection of by-products, the elution was performed in  
285 gradient mode as described as follows: the LC-MS/MS analysis was performed using  
286 LC 20AD XR Shimadzu chromatograph with Shim Pack C-18 reversed-phase as  
287 stationary phase (100 mm × 3.0 mm, 2.2 µm particle size, from Shimadzu<sup>®</sup>) and a  
288 mixture of H<sub>2</sub>O (A) and acetonitrile (B), both acidified with 0.1% formic acid, as  
289 mobile phase. The gradient elution, employed at a flow rate of 0.8 mL min<sup>-1</sup>, was  
290 carried out in the following conditions: 0-5 min: 10-37% B; 5-8 min: 37-100% B; 8-10  
291 min: 100-10% B. The injection volume and column temperature employed were 10 µL  
292 and 26 °C, respectively. The chromatographic system was coupled to 8030-quadrupole  
293 mass spectrometer (Shimadzu, Kyoto, Japan), which operated under an electrospray  
294 interface, in positive mode. The MS/MS conditions applied were as follows: curtain gas  
295 at 20 psi, ion spray at 4000 V, desolvation temperature of 250 °C, and ion source  
296 temperature of 400 °C. Selected ion monitoring (SIM) and full scan experiments were  
297 performed automatically.

298 The calculated value of specific electrical consumption per unit TOC mass  
299 ( $EC_{TOC}$ ) was defined by  $kWh\ g^{-1}\ TOC$ . This value can be derived from Eq. 1, where  
300  $E_{cell}$  is the cell potential (in V),  $I$  is the applied current (in A),  $V$  is the wastewater  
301 volume (in L), and  $\Delta TOC_{exp}$  is the TOC removed (in  $mg\ L^{-1}$ ) at time  $t$  (in h); for the  
302 experiment involving the use of UVC lamp, Eq. 1 is also used considering the electrical  
303 energy associated with the use of lamp, where  $P$  is the nominal power (in W):

$$E_{TOC}(kWh\ g^{-1}TOC) = \frac{E_{cell}Ixt + P t}{V(\Delta TOC)_{exp}} \quad \text{Eq. 1}$$

304 **2.5 Ecotoxicological Assessment**

305 The ecotoxicological effects ( $LC_{50}$ ) of some chlorinated degradation by-products  
306 of TBT in fish (*Fathead minnow*, 96 h) and crustaceans (*Daphnia magna*, 48h) were  
307 predicted/estimated using the Computational Toxicology and Exposure Online  
308 Resources (Comptox) tool. This safe chemical analysis program relies on Quantitative  
309 Structure-Activity Relationship (QSAR) models to estimate toxicity based on the  
310 physical characteristics of the structures and the experimental data obtained from many  
311 reliable sites, databases, sources, including the U.S. Federal and State sources, and  
312 international agencies. For this study, the Toxicity Estimation Software Tool (T.E.S.T)  
313 version 5.1 was used for the analysis of toxicity, since it possesses the highest number  
314 of tests available in the literature with good prediction results [22].

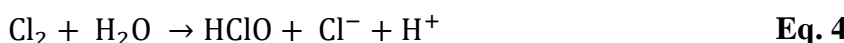
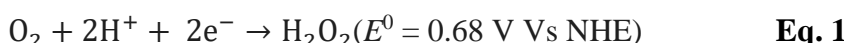
315 **3 Results and Discussion**

316 **3.1 Optimization of Parameters for TBT Degradation**

317 In this section, we evaluated the effect of key operating conditions, such as  
318 current density, added  $Cl^-$  concentration and pH, on the degradation of TBT solution  
319 ( $100\ \mu mol\ L^{-1}$ ) using an EFR operated under the combined system which involved the

320 simultaneous electro-generation of  $\text{H}_2\text{O}_2$  and  $\text{ClO}^-$  in the presence of UVC light. The  
321 optimization of these parameters is fundamentally important because it leads to  
322 significant improvements in TBT degradation efficiency, in addition to minimizing  
323 energy consumption and maximizing the resulting environmental benefits. Operating  
324 under optimized parameters not only improves the performance of the degradation  
325 process, but also provides us with ample metrics for comparing the results of this study  
326 with those reported in the existing literature.

327 Under the UVC/e- $\text{H}_2\text{O}_2$ @e- $\text{ClO}^-$  process, the electrochemical production of  
328  $\text{H}_2\text{O}_2$  and reactive chlorine species is expected to occur through the action mechanism  
329 of suitable cathodes and anodes. At the cathode,  $\text{H}_2\text{O}_2$  is produced through oxygen  
330 reduction reaction via a two-electron mechanism (2e-ORR) (**Eq. 2**)[23]; on the surface  
331 of the DSA<sup>®</sup>- $\text{Cl}_2$  anode, active chlorine (in the form of  $\text{Cl}_2$ ) is generated through  $\text{Cl}^-$   
332 anodic oxidation via **Eq. 3**.  $\text{Cl}_2$  diffusion in the bulk solution can occur  
333 disproportionately to hypochlorous acid (HClO) and  $\text{Cl}^-$ , as shown in **Eq. 4**. In solution,  
334 HClO is in equilibrium with hypochlorite ion ( $\text{ClO}^-$ ), as can be noted in **Eq. 5** [24].



335 It has been well documented that under UVC irradiation,  $\text{H}_2\text{O}_2$  and  $\text{ClO}^-$  can  
336 promote the formation of other stronger reactive agents. For instance, the activation of  
337  $\text{H}_2\text{O}_2$  by UVC leads to the production of hydroxyl radical ( $\text{HO}^\cdot$ ) (**Eq. 6**) (Zhao et al.,

338 2022), while chlorine radical ( $\text{Cl}^{\cdot}$ ) and  $\text{HO}^{\cdot}$  are generated from the homolysis of  $\text{HClO}$   
339 and  $\text{ClO}^{-}$ , as demonstrated in Eq. 7 [25].



340 According to the literature, by increasing the current density ( $j$ ), one enhances  
341 the production of active chlorine on the surface of the DSA<sup>®</sup>- $\text{Cl}_2$  anode [4] and  $\text{H}_2\text{O}_2$  on  
342 GDEs made of PL6C [10,26]. However, a progressive increase of  $j$  during  $\text{H}_2\text{O}_2$   
343 electrogeneration leads to parallel reactions, which are favored at higher overvoltage  
344 (overpotential)[5]. Taking these observations into account, the present study evaluated  
345 the effects of applying different current densities; the current densities evaluated were in  
346 the range of 5 -15 mA cm<sup>-2</sup>, as shown in Fig. 3a.

347 It is worth pointing out that, since the GDE cathode was made of porous carbon  
348 material, a control experiment was performed, without the application of current, in  
349 order to ensure that there was no adsorption of TBT on the electrode; the result of this  
350 experiment showed that there was no decrease in TBT concentration in the system after  
351 90 min of electrolysis.

352  
353 **Fig 3. a)** TBT degradation based on the application of UVC/e- $\text{H}_2\text{O}_2$ @e- $\text{ClO}^{-}$  at  
354 different current densities; **b)** effect of NaCl concentration on TBT degradation; and **c)**  
355 effect of pH on TBT degradation. **Inset:** % of TOC removed from initial solution.

356 The analysis of TBT degradation (Fig. 3a) points to a two-step process. As  
357 shown in Fig. S-1, the first 15 min stage exhibits slow kinetics, while the second stage

358 shows a faster kinetic rate that varies depending on the applied conditions. These  
 359 outcomes are likely linked to the accumulation of oxidants within the system before  
 360 their activation and will be thoroughly discussed in section 3.3. A first-order kinetic  
 361 model fits well for all the curves. The rate constant ( $k$ ,  $\text{min}^{-1}$ ) presented in Table 1 is  
 362 associated with the second step and was obtained from the slope of **Eq. 8**, where  $C_0$  and  
 363  $C$  are the initial and final concentrations ( $\text{mg L}^{-1}$ ) of TBT, respectively, at time  $t$ .

$$\ln \frac{C_0}{C} = k t \quad \text{Eq. 8}$$

364 **Table 1.** Effects of different parameters on TBT degradation and the amount of  
 365 electrical energy consumed in the degradation process.

UVC/e-H <sub>2</sub> O <sub>2</sub> @e-ClO <sup>-</sup>				
Parameter	TBT removal $t_{60\text{min}} (\%)$	$k (\text{min}^{-1})$	$R^2$	TOC Removal $t_{90\text{min}} (\%)$
<b><math>j (\text{mA/cm}^2)</math><sup>a</sup></b>				
15	99.1	$8.556 \cdot 10^{-2}$	0.97	71.2
10	99.4	$8.573 \cdot 10^{-2}$	0.93	62.1
5	95.6	$5.087 \cdot 10^{-2}$	0.91	39.0
<b>NaCl (mM)<sup>b</sup></b>				
15	99.4	$8.573 \cdot 10^{-2}$	0.93	62.1
10	99.5	$8.820 \cdot 10^{-2}$	0.95	63.2
5	99.4	$8.143 \cdot 10^{-2}$	0.91	59.6
<b>pH<sup>c</sup></b>				
3	98.2	$6.361 \cdot 10^{-2}$	0.91	48.2
7	99.5	$8.820 \cdot 10^{-2}$	0.95	63.2

366 Electrolysis condition

367 <sup>a</sup>  $[\text{K}_2\text{SO}_4] = 45 \text{ mM}$ ;  $[\text{Cl}^-] = 15 \text{ mM}$ ;  $\text{pH} = 7.0$

368 <sup>b</sup> current density =  $10 \text{ mA cm}^{-2}$ ;  $\text{pH} = 7.0$

369 <sup>c</sup> current density =  $10 \text{ mA cm}^{-2}$ ;  $\text{Cl}^- = 10 \text{ mM}$

370

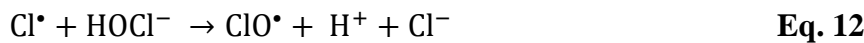
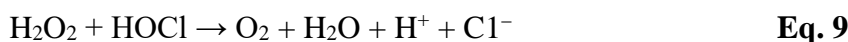
371 The plot in Figure S-1 shows a slow degradation rate in the first 15 min of  
 372 treatment; oxidation occurs faster after this period. This behavior can be observed in all

373 the operating conditions. To understand the reasons behind this variation, it is important  
374 to consider that at the initial stages of the degradation process, the concentration of  
375 oxidants is still increasing. This observation has been made in a previous study  
376 conducted using a PL6C-based GDE in similar conditions [10]. A similar effect is  
377 expected regarding the kinetics involving the generation of active chlorine in DSA<sup>®</sup>-  
378 Cl<sub>2</sub>-type anodes [27].

379 Likewise, increasing *j* also leads to an increase in TOC removal (inset in Fig. 3a  
380 and Table 1). At low current density (5 mA cm<sup>-2</sup>), there is a mild organic compound  
381 remediation (up to 39% of TOC removal), while a greater rate of mineralization is  
382 observed at 10 mA cm<sup>-2</sup> (62.1%) and 15 mA cm<sup>-2</sup> (71.2 %) – all after 90 min of  
383 treatment. Furthermore, the NO<sub>3</sub><sup>-</sup> being monitored, which is a by-product of TBT  
384 degradation, is also favored at the current densities ranging from 10 to 15 mA cm<sup>-2</sup> (see  
385 Fig. S-3a); this shows that higher current densities are more suitable for TBT  
386 mineralization. It should be noted, however, that the presence of NO<sub>3</sub><sup>-</sup> may lead to an  
387 increase in the genotoxicity of the treated solution, apart from inhibiting H<sub>2</sub>O<sub>2</sub>  
388 formation, as reported in other works [28]. Thus, 10 mA cm<sup>-2</sup> was found to be the most  
389 suitable current density, since raising the current density above this limit leads to more  
390 energy consumption and an unwanted increase in NO<sub>3</sub><sup>-</sup> concentration.

391 The effect of added Cl<sup>-</sup> concentration (5-15 mmol L<sup>-1</sup>) - another key parameter  
392 that is expected to influence the concentration of oxidants generated and the efficiency  
393 of the degradation process, was evaluated at the current density of 10 mA cm<sup>-2</sup> and pH  
394 of 7.0 (Fig 3b). In this study, the variation of Cl<sup>-</sup> is reflected in the concentration range  
395 observed in real water matrices ranging from 200 to 500 mg L<sup>-1</sup>, which is equivalent to  
396 between 5.6 and 14 mmol L<sup>-1</sup> [29]. An increase in Cl<sup>-</sup> concentration slightly affects the

397 removal of TBT or TOC. This behavior can be linked to the fact that the excessive  
398 concentration of HClO/ClO<sup>-</sup> can scavenge the HO<sup>•</sup> and Cl<sup>•</sup> generated, as can be seen in  
399 **Eqs. 10-13** [30], and HClO can react with H<sub>2</sub>O<sub>2</sub>, as shown in **Eq. 9**. Moreover, this  
400 effect can be easily observed in Fig. S-2, which presents a comparative analysis of the  
401 electrogeneration of H<sub>2</sub>O<sub>2</sub> in different conditions, in the presence and absence of TBT  
402 and other scavengers (e.g. UVC, HClO/ClO<sup>-</sup>).



403 Regarding the formation of NO<sub>3</sub><sup>-</sup>, the addition of Cl<sup>-</sup> led to a decrease in the  
404 concentration of NO<sub>3</sub><sup>-</sup> detected; this shows that the presence of chlorine affects the  
405 formation of NO<sub>3</sub><sup>-</sup> species (Fig S-3b), probably due to the chlorination of TBT, instead  
406 of its mineralization, as we will see further in this work. Also, an increase in NO<sub>3</sub><sup>-</sup>  
407 formation led to a decrease in H<sub>2</sub>O<sub>2</sub> accumulation. After 90 min of treatment, the  
408 experiments involving the use of an initial concentration of 5, 10 and 15 mM of Cl<sup>-</sup>  
409 generated 2.1, 2.9 and 3.9 mg L<sup>-1</sup> of NO<sub>3</sub><sup>-</sup>, respectively, while the corresponding H<sub>2</sub>O<sub>2</sub>  
410 concentrations produced were 122.9, 98.1 and 75.8 mg L<sup>-1</sup>. In the presence of 10 mmol  
411 L<sup>-1</sup> of Cl<sup>-</sup>, we observed slight improvements in both TBT degradation and NO<sub>3</sub><sup>-</sup>  
412 formation. Based on these results, the current density of 10 mA cm<sup>-2</sup> and the Cl<sup>-</sup>

413 concentration of 10 mmol L<sup>-1</sup> were chosen (constant) for the conduct of subsequent  
414 experiments for the analysis of the effect of pH variation.

415 The effect of initial pH (3.0 and 7.0) on TBT degradation was also evaluated.  
416 Fig. 3c shows that by changing the pH from 3.0 to 7.0, TBT removal is slightly  
417 affected; however, in terms of TOC removal, it is clear that pH 7.0 outperforms pH 3.0.  
418 It is known that in the pH range of 3-7, the predominant active chlorine species is  
419 HClO, and an increase in pH leads to a corresponding increase in ClO<sup>-</sup> ions [31].

420 Looking into the existing literature, one will observe that very few studies have  
421 employed co-generated oxidants in electrochemical systems for water remediation  
422 purposes. Table 2 (indexes 1-3) presents an outline of some studies reported in the  
423 literature where both cathode and anode have been used for the simultaneous production  
424 of oxidant species, in conjunction with UV light, aimed at water remediation. These  
425 studies have commonly employed different cathodes to generate H<sub>2</sub>O<sub>2</sub>, while the anode  
426 has primarily produced chlorine species. The studies presented in indexes 1 and 2  
427 employed low pollutant concentrations (0.1-5.0 mg L<sup>-1</sup>), where they obtained rapid  
428 pollutant removal within minutes of treatment; it should be noted, however, that study 2  
429 required approximately 60 minutes of electrolysis to obtain 57.8% mineralization. In  
430 study 3, an Sb-doped anode produced hydroxyl radicals (HO<sup>•</sup>) which helped promote  
431 the removal of high concentrations of phenol (94 mg L<sup>-1</sup>); the study recorded a complete  
432 contaminant removal after 60 minutes of treatment, though only 40% mineralization  
433 was obtained.

434 While no studies reported in the literature have investigated TBT degradation  
435 using co-generated oxidants, some studies have employed electrochemical systems for  
436 TBT degradation for comparison purposes, as shown in Table 2 (indexes 4-6). These

437 studies employed different electrochemical advanced oxidation processes (EAOP) to  
438 degrade approximately 100 mg L<sup>-1</sup> of TBT. In studies 4 and 5, H<sub>2</sub>O<sub>2</sub> production  
439 occurred at the cathode, while boron-doped diamond (BDD) was used as the active  
440 anode. In study 6, a DSA<sup>®</sup> anode was used to generate Cl<sub>2</sub> (as the oxidant), while an  
441 inactive stainless steel was used as cathode. All the three studies mentioned above  
442 required about 120 minutes of electrolysis to eliminate 100 mg L<sup>-1</sup> of TBT, but  
443 mineralization only occurred after 300 to 540 min of treatment.

444 For comparison purposes, the method proposed in our present study (index 7),  
445 which involved the co-generation of oxidants with UV irradiation, promoted 100% TBT  
446 degradation in 60 min of treatment and a remarkable 63.2% mineralization rate in one-  
447 third of the time reported by the other methods. These results show that the application  
448 of the proposed mechanism, which involved the co-generation of oxidants in the  
449 presence of UV irradiation, significantly enhances the efficiency of electrochemical  
450 systems used in environmental remediation.

451 For a comparison of energy consumption during the degradation process, a  
452 comparative analysis of specific electrical consumption per unit TOC mass was  
453 performed with a view to comparing the amount of energy consumed in the proposed  
454 system with that of the other studies conducted on TBT degradation. As it is evident, the  
455 proposed system required relatively lower amount of energy for TOC removal  
456 compared to the other studies. It is worth noting that with the application of low  
457 pressure Hg lamps (9W UVC in the present study), the amount of energy consumed in  
458 the proposed system was quite low compared to that of other systems in which UVA or  
459 UVC was employed – where high-pressure Hg lamps were mainly applied. In essence,  
460 this is one of the key advantages of the proposed system. Furthermore, the use of highly

461 efficient anodes for the cathodic and anodic formation of oxidants also helps to explain  
 462 the high efficiency of this system compared to other similar systems.

463 **Table 2.** Comparative analysis of different EAOPs applied for contaminants  
 464 degradation in previous studies reported in the literature.

Index	Cathode (oxidant)	Anode (oxidant)	UV irradiation	Contaminant	Degradation	TOC removal	Energy consumption	Ref.
1	C-PTFE (H <sub>2</sub> O <sub>2</sub> )	DSA <sup>®</sup> (Cl <sub>2</sub> )	UV	Ibuprofen, gemfibrozil, naproxen, and diclofenac	84-100 % (after 5.6 min)	-	-	[7]
2	modified graphite felt (H <sub>2</sub> O <sub>2</sub> )	DSA <sup>®</sup> (Cl <sub>2</sub> )	UV	carbamazepine	100 % (after 4 min)	57.8 % (after 60 min)	1.12 kWh/m <sup>3</sup> order <sup>-1</sup>	[32]
3	carbon nanotube (H <sub>2</sub> O <sub>2</sub> )	Sb-doped (HO <sup>•</sup> )	-	Phenol	100 % (after 60 min)	40 % (after 60 min)	0.12 kWh g-TOC <sup>-1</sup>	[6]
4	carbon-PTFE air-diffusion (H <sub>2</sub> O <sub>2</sub> )	BDD	UVA	Tebuthiuron	100 % (after 180 min)	>90 % (after 540 min)	-	[33]
5	GDE (H <sub>2</sub> O <sub>2</sub> )	BDD	UVC	Tebuthiuron	87.9 % (after 120 min)	~95 % (after 360 min)	~45 kWh m <sup>-3</sup> order <sup>-1</sup>	[26]
6	stainless steel	DSA <sup>®</sup> (Cl <sub>2</sub> )	UVC	Tebuthiuron	100 % (after 120 min)	100 % (after 300 min)	3.0 kW h g <sup>-1</sup> TOC	[24]
7	GDE (H <sub>2</sub> O <sub>2</sub> )	DSA <sup>®</sup> (Cl <sub>2</sub> )	UVC	Tebuthiuron	100 % (after 60 min)	63.2 % (after 90 min)	1.5 kWh g <sup>-1</sup> TOC	This work

465

### 466 3.2 Contributory Effect of Combined EAOPs Applied in TBT Degradation

467 The combined UVC/e-H<sub>2</sub>O<sub>2</sub>@e-ClO<sup>-</sup> process exhibited a good performance  
 468 when applied for TBT degradation under optimized experimental conditions (i.e., 10  
 469 mA cm<sup>-2</sup>; 10 mmol L<sup>-1</sup> of Cl<sup>-</sup>; and pH 7); however, to better understand the contribution  
 470 of each system in the degradation process, control experiments were performed using  
 471 the following processes: photolysis (UVC), anodic oxidation (AO), e-H<sub>2</sub>O<sub>2</sub>, e-ClO<sup>-</sup>,  
 472 UVC/e-H<sub>2</sub>O<sub>2</sub>, UVC/e-ClO<sup>-</sup>, and UVC/e-H<sub>2</sub>O<sub>2</sub>@e-ClO<sup>-</sup>. Fig. 4 shows the results  
 473 obtained from the comparative analysis of different EAOPs applied for TBT  
 474 degradation; the results show the contribution of each process in the contaminant

475 removal and mineralization. In addition, the TOC results were used to calculate the  
476 contribution of each process and the energy costs involved, as described in **Eq. 1**.

477

478 **Fig. 4.** **a)** TBT degradation curve; **b)** TOC removal after 90 min of treatment; **c)**  
479 Contribution of each process in TOC removal; **d)** Electrical energy consumed per gram  
480 of TOC removed, based on the application of different EAOPs investigated in this  
481 study.

482 The TBT degradation curves obtained from the application of the different  
483 treatment systems are presented in Fig. 4a. As can be noted, three processes exhibited  
484 the most efficient results in terms of TBT degradation: i) UVC/e-H<sub>2</sub>O<sub>2</sub>; ii) UVC/e-ClO<sup>-</sup>  
485 – each electrogenerated oxidant in the presence of UVC; and iii) the combined UVC/e-  
486 H<sub>2</sub>O<sub>2</sub>@e-ClO<sup>-</sup> process. Among these three processes, the combined UVC/e-H<sub>2</sub>O<sub>2</sub>@e-  
487 ClO<sup>-</sup> system exhibited the best degradation rate, recording 99.0% TBT degradation in  
488 60 min of treatment; this was followed by UVC/e-H<sub>2</sub>O<sub>2</sub> and UVC/e-ClO<sup>-</sup> with 97.3 and  
489 89.7% degradation rates, respectively, for the same treatment time. Yin H. et al. (2021)  
490 obtained similar results when they studied the use of activated electrogenerated chlorine  
491 and H<sub>2</sub>O<sub>2</sub> in the presence of UV for the degradation of different contaminants; in their  
492 study, the combined UV/E-Cl&H<sub>2</sub>O<sub>2</sub> system also exhibited the best performance in  
493 terms of contaminants removal compared with UV/E-Cl and UV/E-H<sub>2</sub>O<sub>2</sub>. In the  
494 aforementioned study conducted by Yin et al. (2021), the authors also found that the  
495 combined UV/e-Cl&H<sub>2</sub>O<sub>2</sub> system exhibited superior performance when they tested  
496 different water matrices (including lake water, secondary wastewater effluent, and  
497 medical wastewater); this clearly points to the versatility of the combined system, as it  
498 can be employed for a wide range of purposes [32].

499 To better evaluate the ability of each EAOP to remove organic matter in the  
500 system, TOC analysis was used to estimate the rate of mineralization (see Fig. 4b). This  
501 approach allows one to have a better understanding of the process involving the  
502 decontamination of the by-products formed after the target compound has been  
503 eliminated. For this analysis, the electrolysis lasted 90 min. Once again, the UVC/e-  
504  $\text{H}_2\text{O}_2@\text{e-ClO}^-$  system exhibited the best performance; it recorded 63.2% TOC removal  
505 in 90 min. An interesting result was observed in terms of TOC removal when the  
506 process containing only  $\text{H}_2\text{O}_2$ (AO-e- $\text{H}_2\text{O}_2$  and UVC/e- $\text{H}_2\text{O}_2$ ) was compared with that  
507 containing only chlorine (AO-e- $\text{ClO}^-$  and UVC/e- $\text{ClO}^-$ ). After 90 min of electrolysis,  
508 the AO-e- $\text{H}_2\text{O}_2$  processes recorded 14.2% TBT degradation (Fig. 4-a), with 9.5% TOC  
509 removal (Fig. 4-b); however, with the addition of UVC, these values increased to 99.8%  
510 (TB degradation) and 51.2% (TOC removal), respectively. The AO-e- $\text{Cl}^-$  process  
511 recorded a better TBT degradation rate (31.4%), but with low TOC removal (3.5%);  
512 interestingly, the combination of the system with UVC (UVC/e- $\text{Cl}^-$ ) resulted in 99.4%  
513 TBT degradation, with 26.3% TOC removal. These results show that chlorine species  
514 exert a more significant effect on TBT degradation (this is probably related to the  
515 chlorination of the molecule), whereas  $\text{H}_2\text{O}_2$  exerts a more significant effect on TOC  
516 removal (which is probably related to high oxidation of  $\text{HO}^\cdot$  radical).

517 To separate the contribution of the EAOP technology in TOC removal, we  
518 subtracted the contribution values derived from the AO and UVC (obtained from  
519 control experiments) from the values recorded for the combined processes: AO-e- $\text{H}_2\text{O}_2$ ,  
520 AO-e- $\text{ClO}^-$ , UVC/e- $\text{H}_2\text{O}_2$ , UVC/e- $\text{ClO}^-$ , and UVC/e- $\text{H}_2\text{O}_2@\text{e-ClO}^-$ . The results  
521 obtained are presented in Fig. 4c; as can be observed, UVC exerts a much higher  
522 contribution (17.3 %) in TOC removal compared to AO (2.9 %). As expected, UVC  
523 irradiation also exerts a significant effect on  $\text{H}_2\text{O}_2$  and  $\text{ClO}^-$  by producing  $\text{HO}^\cdot$  and

524 radical chlorine species (RCS)[24]. After subtracting the effect of UVC and AO from  
525 the other conditions, one can clearly see the synergistic effects. The value of TOC  
526 removal recorded for the UVC/e-H<sub>2</sub>O<sub>2</sub> and UVC/e-ClO<sup>-</sup> processes was 31.0% and  
527 6.13%, respectively. For the combined process (UVC/e-H<sub>2</sub>O<sub>2</sub>@e-ClO<sup>-</sup>), the rate of TOC  
528 removal derived from RCS and HO<sup>•</sup> only was 39.8%, which is approximately the sum of  
529 the values recorded for the UVC/e-H<sub>2</sub>O<sub>2</sub> and UVC/e-ClO<sup>-</sup> processes. Thus, the  
530 combined UVC/e-H<sub>2</sub>O<sub>2</sub>@e-ClO<sup>-</sup> system recorded an increase of 8.8% in TOC removal  
531 compared to UVC-e-H<sub>2</sub>O<sub>2</sub> – the second highest.

532 Other works reported in the literature have shed light on the role of the  
533 combined treatment processes, and have pointed out their contribution to the treatment  
534 of a wide range of pollutants [32]. Zhang et al. (2022) obtained interesting results in  
535 their study on the use of ultraviolet irradiation with electrochemical chlorine and  
536 hydrogen peroxide production for the degradation of gemfibrozil, ibuprofen, and  
537 naproxen; in this study, the authors found that the combined application of UV and  
538 electrogenerated Cl<sub>2</sub> produced efficient results in terms of gemfibrozil and naproxen  
539 degradation, but the technique proved ineffective for the degradation of ibuprofen. By  
540 contrast, the e-UV/H<sub>2</sub>O<sub>2</sub> process yielded effective results in terms of ibuprofen removal,  
541 yet was less effective for gemfibrozil and naproxen removal.

542 The amount of energy consumed (E<sub>TOC</sub>) based on the contribution of each EAOP  
543 system is presented in Fig. 4d. The E<sub>TOC</sub> value was calculated based on the analysis of  
544 TBT (100  $\mu\text{mol L}^{-1}$ ) and by-products degradation after 90 min of electrolysis, where  
545 63.2% removal was recorded. The effect of TBT degradation observed in the  
546 experiment conducted using only UVC served as a reference for separating the amount  
547 of energy consumed by the electrochemical reactor. The UVC system exhibited higher  
548 levels of energy consumption, with UVC/e-H<sub>2</sub>O<sub>2</sub>, UVC/e-ClO<sup>-</sup> and UVC/e-H<sub>2</sub>O<sub>2</sub>@e-

549  $\text{ClO}^-$  recording 1.7, 3.5 and 1.5  $\text{kWh g}^{-1}$  TOC, respectively. Gozzi et al. (2017)  
550 employed a flow plant of 2.5 L, equipped with a boron-doped diamond (BDD)/air-  
551 diffusion cell and a solar planar photoreactor, to degrade 0.18 mmol tebuthiuron using  
552 anodic oxidation combined with the following different processes: electrogenerated  
553  $\text{H}_2\text{O}_2$  (AO- $\text{H}_2\text{O}_2$ ), electro-Fenton (EF) and solar photoelectro-Fenton (SPEF); based on  
554 the results of the study, the EF and SPEF processes yielded the best results – EF: energy  
555 consumption of 1.0  $\text{kWh g}^{-1}$  TOC, current density of  $25 \text{ mA cm}^{-2}$ , and 42% TOC  
556 removal; SPEF: energy consumption of 0.41  $\text{kWh g}^{-1}$  TOC, current density of 50  $\text{mA}$   
557  $\text{cm}^{-2}$ , and 41% TOC removal. In our present study, the high energy consumption  
558 recorded for all the systems that involved the use of UVC can be attributed to the Hg  
559 lamp (254 nm), which consumes  $9 \text{ W h}^{-1}$ , since the maximum amount of energy  
560 consumed by the electrochemical reactor in the UVC/e- $\text{H}_2\text{O}_2$ @e- $\text{ClO}^-$  system was only  
561 0.12  $\text{kWh g}^{-1}$  TOC.

562 *3.3 Role of  $\text{HO}^\bullet$  Species in TBT Degradation*

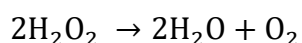
563 Based on the results presented in the previous sections, it is clear that the  
564 UVC/e- $\text{H}_2\text{O}_2$  and UVC/e- $\text{H}_2\text{O}_2$ @e- $\text{ClO}^-$  processes exhibited high efficiency when  
565 applied for TBT degradation. This observed effect can be directly attributed to the  
566 generation of  $\text{HO}^\bullet$  species from the photolysis of the electrogenerated  $\text{H}_2\text{O}_2$  and  $\text{ClO}^-$ .  
567 Thus, electrolysis tests were carried out using salicylic acid (Sac. Ac.), a well known  
568 scavenger of  $\text{HO}^\bullet$ , in order to determine the role of  $\text{HO}^\bullet$  species in each treatment  
569 process [34–36]. It is worth mentioning that the rate constant related to the  
570 hydroxylation reaction of Sac. Ac. in 2,5-DHBA is slightly higher than that of 2,3-  
571 DHBA ( $2.4 \times 10^{10} \text{ L mol}^{-1} \text{ s}^{-1}$  vs.  $1.3 \times 10^{10} \text{ L mol}^{-1} \text{ s}^{-1}$ ) [34]. The decomposition of Sac.  
572 Ac. and the formation of the intermediate dihydroxybenzoic acid (DHBA) are shown in  
573 Fig. 5, for all the processes involving  $\text{H}_2\text{O}_2$  (i.e., AO/e- $\text{H}_2\text{O}_2$ , UVC/e- $\text{H}_2\text{O}_2$ , and UVC/e-

574  $\text{H}_2\text{O}_2@\text{e-ClO}^-$ ). Control experiments were also conducted using only AO and  
575 photolysis (UVC) in order to evaluate the effects of these processes on the degradation  
576 of Sac. Ac. and on the formation of its intermediates (Fig. S-4).

577

578 **Fig. 5.** Analysis of salicylic acid (Sac. Ac.) and 2,3- and 2,5-dihydroxybenzoic acid  
579 (DHBA) degradation as a function of time, based on the application of the following  
580 treatment systems: **a)** AO/e- $\text{H}_2\text{O}_2$ ; **b)** AO/e- $\text{H}_2\text{O}_2@\text{e-ClO}^-$ ; **c)** UVC/e- $\text{H}_2\text{O}_2$ ; **d)** UVC/e-  
581  $\text{H}_2\text{O}_2@\text{e-ClO}^-$ .

582 As expected, the AO/e- $\text{H}_2\text{O}_2$  system recorded low  $\text{HO}^\bullet$  production (Fig. 5a),  
583 since the activation of  $\text{H}_2\text{O}_2$  has very slow kinetics in the absence of UVC radiation  
584 [37]. It is also worth noting that  $\text{H}_2\text{O}_2$  can be decomposed into  $\text{H}_2\text{O}$  and  $\text{O}_2$  at standard  
585 temperature and pressure (see **Eq. 14**).



**Eq. 14**

586 After 90 min of electrolysis under the AO/e- $\text{H}_2\text{O}_2$  system, the concentration of  
587 2,5-DHBA was found to be approximately  $1.1 \text{ mg L}^{-1}$  ( $\sim 7.1 \mu\text{mol L}^{-1}$ ); despite the low  
588 degradation value recorded, the presence of  $\text{HO}^\bullet$  explains the good rate of TOC removal  
589 (9.5%) obtained compared to the other systems that had no UVC. It should be noted that  
590 although the AO/e- $\text{H}_2\text{O}_2@\text{e-ClO}^-$  condition (Fig. 5b) was not tested in TBT  
591 degradation, it helps explain the role of chlorine electrogenerated species in the system  
592 – through the scavenger test. The AO/e- $\text{H}_2\text{O}_2@\text{e-ClO}^-$  system recorded a decrease of  
593  $17.8 \text{ mg L}^{-1}$  in Sac. Ac. concentration after 90 min of electrolysis; essentially, this is  
594 more than five times higher than that recorded for the AO/e- $\text{H}_2\text{O}_2$  system. The 2,5-  
595 DHBA concentration was found to be  $1.5 \text{ mg L}^{-1}$  under the AO/e- $\text{H}_2\text{O}_2@\text{e-ClO}^-$

596 system; this value is quite close to that recorded for the AO/e-H<sub>2</sub>O<sub>2</sub> system (Fig. 5a).  
597 This result, related to the formation of 2,5-DHBA, is found to be consistent with the  
598 AO/e-ClO<sup>-</sup> system, which shows 33.7% of TBT degradation, but only 3.5% of TOC  
599 removal (see Fig. 4a-b). Importantly, these findings show that chlorine species favor the  
600 removal of contaminants, while hydroxyl radical favor TOC reduction.

601 In systems with UVC light, Sac. Ac. degradation is found to be more  
602 pronounced than in those without irradiation; this can be observed from the results  
603 obtained for the UVC/e-H<sub>2</sub>O<sub>2</sub> and UVC/e-H<sub>2</sub>O<sub>2</sub>@e-ClO<sup>-</sup> systems shown in Figs. 5d-c.  
604 In the control tests (Fig. S-4), one will observe that there is a decrease in Sac. Ac.  
605 concentration in the presence of only UVC light, but no intermediates are detected; this  
606 is attributed to the photolysis of the Sac. Ac. molecule and not to the effect of the HO<sup>·</sup>  
607 species. Thus, it is necessary to keep in mind that in all the processes in which UVC is  
608 incorporated, a small portion of the decrease in Sac. Ac. is caused by the photolysis of  
609 the molecule.

610 As observed in the UVC/e-H<sub>2</sub>O<sub>2</sub> and UVC/e-H<sub>2</sub>O<sub>2</sub>@e-ClO<sup>-</sup> processes (Fig 5d-  
611 c), detecting the presence of 2,3 and 2,5-DHBA implies that HO<sup>·</sup> species have been  
612 generated and are acting in the hydroxylation of Sac. Ac. The UVC/e-H<sub>2</sub>O<sub>2</sub> system  
613 exhibited the formation of 2,3- and 2,5-DHBA, which apparently presented a plateau  
614 concentration after 60 min of electrolysis, reaching 10.1 and 7.3 mg L<sup>-1</sup>, respectively, in  
615 90 min. These results explain why the UVC/e-H<sub>2</sub>O<sub>2</sub> system recorded excellent TBT  
616 removal and degradation rates (Fig. 4a-b). As can be noted, between 60 and 90 min of  
617 electrolysis, the TBT degradation rate changes very little (97.3 and 99.8%,  
618 respectively); however, the TOC removal rate doubles from 23.4 to 51.2%. Essentially,  
619 the results show that HO<sup>·</sup> plays an important role in TBT degradation (see Fig. 4a-b).

620 Another interesting observation that is worth mentioning is that the results  
621 obtained for the UVC/e-H<sub>2</sub>O<sub>2</sub>@e-ClO<sup>-</sup> system (Fig. 5d) provide insights into the  
622 generation of RCS in that system rather than only HO<sup>•</sup> species. In 60 min of electrolysis,  
623 the concentration of 2,3 and 2,5-DHBA reached a plateau at 8.7 and 6.8 mg L<sup>-1</sup>,  
624 respectively; within the span of this time, the TBT degradation and TOC removal rates  
625 recorded were 98.9% and 32.6%, respectively (see Fig. 4a-b). However, after 60 min of  
626 electrolysis, a decrease was observed in the concentration of both 2,3- and 2,5-DHBA  
627 compounds; this explains the preferred pathway of RCS, which is aimed at removing  
628 other compounds rather than mineralizing them.

629 It is worth highlighting that despite the role played by HO<sup>•</sup>, other mechanisms  
630 are involved in the UVC/e-H<sub>2</sub>O<sub>2</sub>@e-ClO<sup>-</sup> process applied for TBT degradation (Fig. 6).  
631 The degradation of TBT in water also occurs via the action of reactive chlorine species  
632 (e.g. Cl<sub>2</sub>, HClO/ClO<sup>-</sup> and Cl<sup>•</sup>), as previously explained here. These RCS species are  
633 together responsible for the conversion of TBT into intermediates and/or inorganic ions,  
634 which leads to the partial mineralization of the molecule. For the mineralization process,  
635 a minor contribution is also expected from direct oxidation and UVC photolysis.

636  
637 **Fig. 6.** Schematic diagram of possible TBT degradation mechanisms under the UVC/e-  
638 H<sub>2</sub>O<sub>2</sub>@e-ClO<sup>-</sup> system.

639  
640 *3.4 Possible Pathway of TBT Degradation*

641 To better understand the role of e-H<sub>2</sub>O<sub>2</sub> and e-ClO<sup>-</sup> oxidants combined with  
642 UVC irradiation in TBT degradation, the degradation by-products generated in the most  
643 efficient systems (UVC/e-H<sub>2</sub>O<sub>2</sub>, UVC/e-ClO<sup>-</sup>, and UVC/e-H<sub>2</sub>O<sub>2</sub>@e-ClO<sup>-</sup>) were  
644 detected and identified through LC-MS/MS analyses. The mass spectra of the

645 intermediates were recorded, and their structures were proposed through the analysis of  
646 the protonated ions  $[M+H]^+$  and fragmentation patterns. As reported in the literature, the  
647 mass spectrum of TBT (molecular weight 228 Da) shows a protonated ion  $[M+H]^+$ , with  
648  $m/z$  229 and a fragment with  $m/z$  172 [38]. Other fragments resulting from the cleavage  
649 between nitrogen and the carbonyl group include the thiadiazole ring (see Fig S-5).

650 The LC-MS chromatograms obtained for the UVC/e- $H_2O_2$ , UVC/e- $ClO^-$  and  
651 UVC/e- $H_2O_2@e-ClO^-$  systems revealed the presence of 17 main intermediates in TBT  
652 degradation. This outcome was anticipated, given that the degradation curves and TOC  
653 analysis exhibited distinct responses for the three systems, as discussed in the previous  
654 section. Table S-1 presents the 17 intermediates recorded in the process involving the  
655 degradation of TBT under the specified systems. Based on the identified intermediates,  
656 four pathways for TBT degradation were proposed; these pathways are presented in Fig.  
657 7.

658  
659 **Fig. 7.** Possible pathways for TBT degradation based on the application of the UVC/e-  
660  $H_2O_2$  (navy blue arrow), UVC/e- $ClO^-$  (red arrow) and UVC/e- $H_2O_2@e-ClO^-$  (light blue  
661 arrow) systems.

662 Pathway 1 begins with the hydroxylation of the 1,3-dimethylurea group of TBT,  
663 which generates intermediate **1** with  $m/z$  245. The validity of this route is corroborated  
664 by the presence of the fragment with  $m/z$  172, corresponding to 5-*tert*-butyl-N-methyl-  
665 1,3,4-thiadiazol-2-amine. The hydroxylated product **1** undergoes oxidation, giving rise  
666 to compound **2**, which is characterized by a molecular ion with  $m/z$  243 and  $m/z$  265  
667  $[M+Na]^+$ . Compound **3** ( $m/z$  229) is derived from the demethylation of compound **2**,  
668 which likely occurs through the oxidation of the methyl group in the urea group,

669 transforming it into a methylene group, followed by the hydrolysis and the loss of the  
670 formyl group ( $\text{H}_2\text{C}=\text{O}$ )[33,38,39].

671 The elimination of the terminal formaldehyde group in intermediate 2 is the  
672 proposed pathway for the formation of compound **4** with  $m/z$  215 [38,39]. Compound **4**  
673 then undergoes the following processes: (i) hydroxylation of the central methyl,  
674 resulting in product **7** with  $m/z$  231; subsequent hydroxylation in the *tert*-butyl group of  
675 compound **4** generates the derivative compound **8** ( $m/z$  279); and (ii) cleavage of the N-  
676 C bond of the urea group, with the release of formamide, gives rise to compound **5** ( $m/z$   
677 172) [24,33,39]. The subsequent oxidation of the methyl substituent of N to alcohol in  
678 compound **5** gives rise to derivative compound **6** with  $m/z$  174 [33].

679 A second identified degradation route (Pathway 2) begins with the hydroxylation  
680 of the central methyl group of TBT, which gives rise to compound **9** with  $m/z$  245. This  
681 compound was identified based on the characteristic fragment with  $m/z$  188, which is  
682 indicative of the rearrangement of primary amides described by McLafferty [24,39].  
683 The hydroxylation of the *tert*-butyl group in compound **9**, followed by the subsequent  
684 oxidation of the alcohol substituent of N to an aldehyde, results in the formation of  
685 product **10** with  $m/z$  291 [24].

686 A third possible TBT degradation route (Pathway 3) involves the hydroxylation  
687 of the *tert*-butyl group of TBT, which leads to the formation of compound **11** ( $m/z$  245).  
688 The hydroxylation of the alkane group has been reported in studies on TBT degradation,  
689 with the characteristic fragment being  $m/z$  184[38,39]. During the electrolysis  
690 conducted in the presence of  $\text{Cl}^-$ , we identified intermediate compounds **12** ( $m/z$  265)  
691 and **13** ( $m/z$  284), which are derived from organochlorination reactions. In compound  
692 **12**, chlorination occurs in the methyl of the *tert*-butyl group due to the higher reactivity  
693 of hydrogen atoms in alkanes. The conditions applied in the electrolysis can also induce

694 chlorination in the nitrogen of the amide group, leading to the formation of product **13**  
695 [24].

696 Pathway 4 is proposed based on the degradation and chlorination of the TBT  
697 molecule. Intermediate compound **14** (*m/z* 215) is derived from the elimination of a  
698 methyl group from the central nitrogen of the urea group. Degradation products **4** and  
699 **14** (both with *m/z* 215) have been previously reported in studies on TBT degradation;  
700 their structures were differentiated by the presence of fragments with *m/z* 172 and *m/z*  
701 158, corresponding to the loss of formamide (45 Da) and methylformamide (59 Da),  
702 respectively [38]. Successive demethylations, chlorinations and hydrolysis of compound  
703 **14** generated the intermediates **15** (*m/z* 227), **16** (*m/z* 213), and **17** (*m/z* 199).

704 The proposed chemical structures indicate the following (Fig. 7; Table S-1): (i)  
705 in the processes involving the presence of peroxide ions in the treated solution,  
706 degradation products are formed through hydroxylation, oxidation and elimination  
707 reactions; (ii) in chlorine-involved processes, hydroxylation and oxidation of the methyl  
708 group (intermediates **1**, **2**, **3**, **6-13**) are not observed, but one is able to identify the  
709 intermediates derived from the cleavage of TBT molecules and the organochlorinated  
710 compounds generated through the attack by  $\text{Cl}^-$  species on the anode surface or by  
711 electrogenerated active chlorine species; (iii) the electrolysis conducted in the presence  
712 of both chlorine and peroxide ions in the treated solution was the only process that led  
713 to the generation of hydroxylated organochlorine intermediates (**12** and **13**).

714 *3.5 Toxicity Assessment of TBT and its Degradation By-products*

715 Studies on the removal of organic pollutants from water commonly focus on the  
716 elimination of the target substance. However, assessing the degradation by-products and  
717 their toxicity is equally vital, as these substances can also negatively impact the  
718 environment. Chlorinated derivatives have been specifically demonstrated to exhibit

719 potential toxicity [40]; hence, in this study, a prediction analysis was conducted using  
720 the Comptox tool to evaluate and predict the ecotoxicity profile of chlorinated TBT by-  
721 products.

722 The Globally Harmonized System of Classification and Labeling of Chemical  
723 Products (GHS) determines the classification of a substance based on its potential  
724 hazard to the aquatic environment. This classification relies on the following: acute  
725 toxicity data, such as lethal concentration 50% (LC<sub>50</sub>) or effective concentration 50%  
726 (EC<sub>50</sub>); and chronic toxicity data, including no observed effect concentration  
727 (NOEC)[41].

728 While experimentally derived test data are preferred, validated quantitative  
729 structure-activity relationships (QSARs) for aquatic toxicity are accepted in the GHS  
730 classification process [41]. GHS defines three categories for acute toxicity (very toxic,  
731 toxic, and harmful), while for chronic toxicity, the same three acute categories are  
732 employed together with category 4, which is associated with long-lasting harmful  
733 effects. The classification relies on NOEC, or equivalent EC<sub>x</sub> data, in conjunction with  
734 data on the degradability of the target substance, along with data on the bio-  
735 concentration factor (BCF) or the n-octanol and water partition coefficient (K<sub>ow</sub>). Table  
736 3 presents the LC<sub>50</sub> values recorded for fish (*Fathead minnow*) and crustaceans  
737 (*Daphnia magna*), along with the BCF with log K<sub>ow</sub>, for all the 17 by-products  
738 intermediates formed during TBT degradation.

739 **Table 3.** Results obtained from the analysis of ecotoxicity (LC<sub>50</sub>) in fish and *Daphnia*  
740 *magna*, along with physical-chemical parameters recorded for TBT degradation by-  
741 products.

Compound	LC <sub>50</sub> (mgL <sup>-1</sup> )	BCF	Log K <sub>ow</sub>
----------	---------------------------------------	-----	---------------------

	<i>Fathead minnow</i> (96 h)	<i>Daphnia magna</i> (48h)		
<b>1</b>	59.1	64.80	4.00	1.05
<b>2</b>	22.98	18.87	8.00	1.79
<b>3</b>	21.9	49.41	5.87	1.46
<b>4</b>	80.99	14.24	4.64	1.40
<b>5</b>	56.67	18.52	11.21	1.80
<b>6</b>	78.52	28.98	7.98	1.14
<b>7</b>	99.63	55.18	3.62	0.42
<b>9</b>	58.67	58.62	3.61	1.00
<b>8</b>	18.84	52.90	3.34	1.34
<b>10</b>	13.72	58.69	2.26	1.64
<b>11</b>	44.24	42.95	3.72	0.94
<b>12</b>	61.93	48.15	4.64	0.91
<b>13</b>	22.05	14.84	5.92	1.37
<b>14</b>	61.13	29.41	4.75	1.53
<b>15</b>	50.55	73.87	8.81	0.86
<b>16</b>	43.75	52.72	9.29	0.64
<b>17</b>	43.02	23.82	20.77	0.56

742

743 The LC<sub>50</sub> values obtained for *Fathead minnow* and *Daphnia magna* were within  
 744 the range of 10.0 < LC<sub>50</sub> ≤ 100; this shows that the substances belong to the acute  
 745 category 3, which is classified as harmful to aquatic life. Regarding the chronic  
 746 ecotoxicity data, the LC<sub>50</sub> values, along with BCF ≥ 500, and/or if absent, log K<sub>ow</sub> ≥ 4  
 747 show that these compounds fall in the chronic toxicity 3 classification, which means  
 748 they are harmful to aquatic life, with long-lasting effects. Although these results  
 749 indicate the presence of hazardous substances in the water after treatment, the  
 750 chlorinated derivatives formed are less toxic than TBT, which is classified under the  
 751 GHS hazard classification framework as category 1; i.e., it is very toxic to aquatic life,  
 752 with short and long-lasting effects [33]. Despite their low toxicity effects, chlorinated  
 753 by-products may pose potential risks even in low concentrations. Interestingly, a review  
 754 of the toxicological aspects of water treated using chlorine-based advanced oxidation  
 755 processes concluded that the toxicity effect can be managed through some experimental

756 parameters [42]. For us to have a more comprehensive understanding of the toxicity of  
757 chlorine by-products, further in-depth analyses are needed.

758         Although the EAOP system proposed in this study reduced the acute toxicity  
759 levels of TBT, it is quite difficult to compare it with other results, as very few studies  
760 have performed acute toxicity analyses using electrochemistry-based systems for TBT  
761 degradation [43–45]. Only one study was found regarding TBT decontamination, which  
762 presented toxicity results after a multi-stage treatment involving coagulation-  
763 flocculation-settling and a photo-Fenton process; in the aforementioned study, the  
764 authors employed *Vibrio fischeri* inhibition tests for the assessment of acute toxicity,  
765 where they observed a reduction in toxicity from 100% to 43% after treatment [46]. In  
766 this regard, the present study brings novel contributions to the fore by performing  
767 toxicity tests for by-products formed during TBT degradation using an EAOP system.

768

#### 769         **4 Conclusion and Future Perspectives**

770         This work demonstrated the effectiveness of the UVC/e-H<sub>2</sub>O<sub>2</sub>@e-ClO<sup>−</sup> system  
771 for TBT degradation and mineralization in an electrochemical flow reactor. Based on  
772 the findings, the following conclusions can be drawn:

773             •         Under the best experimental conditions (10 mA cm<sup>−2</sup>, 10 mmol L<sup>−1</sup> Cl<sup>−</sup>,  
774 and pH 7), the TBT molecule was almost completely degraded, where a degradation  
775 rate of 99.5% was recorded in only 60 min of treatment. In addition, over 63.0% TOC  
776 removal was obtained in 90 min.

777             •         The combined UVC/e-H<sub>2</sub>O<sub>2</sub>@e-ClO<sup>−</sup> process was found (estimated) to  
778 consume low amount of energy (about 1.54 kWh g<sup>−1</sup> TOC). The co-generation of

779 oxidants from both electrodes significantly enhanced TBT mineralization, leading to an  
780 increase of 8.8% in efficiency compared to the individual systems.

781 • HO<sup>•</sup> and chlorine species were identified as the main reactive species  
782 involved in the TBT degradation mechanism. Also, a total of 17 by-products were  
783 detected, and four degradation pathways were proposed.

784 • The results obtained from the ecotoxicity estimations conducted suggest  
785 that the by-products generated in the TBT degradation process were less toxic than  
786 TBT, though they were still harmful to aquatic life. However, it is worth emphasizing  
787 that, while QSAR analyses provide valuable initial estimates of acute and chronic  
788 toxicity, the toxicological responses of the treated matrix should be experimentally  
789 assessed in future studies for us to have a more comprehensive understanding of the  
790 toxicity of TBT degradation by-products.

791 Finally, the pollutant treatment method investigated in this work offers an  
792 alternative approach for using electrical energy more efficiently in EAOPs, as the  
793 simultaneous activation of oxidants generated at both the cathode and anode enhances  
794 the degradation of organic contaminants under UV light. In addition, the treatment  
795 approach implemented in the present study sought to explore the fundamental aspects  
796 involving the application of electrochemical flow reactors and the underlying technical  
797 feasibility. The findings of the study provide a proof of concept that can be scaled up for  
798 industrial applications and bring useful contributions to the fore on the ongoing research  
799 on pollutants degradation.

800

801 **Acknowledgements**

802 The authors acknowledge the financial assistance provided by the Brazilian research  
803 funding agencies, including the Brazilian National Council for Scientific and  
804 Technological Development – CNPq (grant #303943/2021-1), São Paulo Research  
805 Foundation - FAPESP (grants #2018/22210-0, #2018/22211-7, #2018/22022-0,  
806 #2019/06650-3, #2016/19612-4, #2020/02743-4 and #2022/12895-1), and the  
807 University of the State of Mato Grosso (UNEMAT) in support of this research.

808 **Declaration of Competing Interest**

809 The authors declare that they have no known competing financial interests or  
810 personal relationships that could have appeared to influence the work reported in this  
811 paper.

812 **5 References**

- 813 [1] I. Sirés, E. Brillas, M.A. Oturan, M.A. Rodrigo, M. Panizza, Electrochemical  
814 advanced oxidation processes: today and tomorrow. A review, Environmental  
815 Science and Pollution Research 21 (2014) 8336–8367.  
816 <https://doi.org/10.1007/s11356-014-2783-1>.
- 817 [2] A.J. dos Santos, E.C.T. de A. Costa, D.R. da Silva, S. Garcia-Segura, C.A.  
818 Martínez-Huitle, Electrochemical advanced oxidation processes as decentralized  
819 water treatment technologies to remediate domestic washing machine effluents,  
820 Environmental Science and Pollution Research 25 (2018) 7002–7011.  
821 <https://doi.org/10.1007/s11356-017-1039-2>.
- 822 [3] O. Garcia-Rodriguez, E. Mousset, H. Olvera-Vargas, O. Lefebvre,  
823 Electrochemical treatment of highly concentrated wastewater: A review of  
824 experimental and modeling approaches from lab- to full-scale, Crit Rev Environ  
825 Sci Technol 52 (2022) 240–309.  
826 <https://doi.org/10.1080/10643389.2020.1820428>.
- 827 [4] F.C. Moreira, R.A.R. Boaventura, E. Brillas, V.J.P. Vilar, Electrochemical  
828 advanced oxidation processes: A review on their application to synthetic and real  
829 wastewaters, Appl Catal B 202 (2017) 217–261.  
830 <https://doi.org/10.1016/j.apcatb.2016.08.037>.
- 831 [5] S.A. Bueno, G. de Oliveira Santiago Santos, T. Oliveira Silva, M.R. Vasconcelos  
832 Lanza, P. Balderas Hernández, G. Roa Morales, J. Ibáñez Cornejo, C. Sáez, M.A.  
833 Rodrigo, Sustainable integrated process for cogeneration of oxidants for VOCs

834 removal, Chemosphere 342 (2023) 140171.  
835 <https://doi.org/10.1016/j.chemosphere.2023.140171>.

836 [6] S.Y. Yang, H.W. Jeong, B. Kim, D.S. Han, W. Choi, H. Park, Electrocatalytic  
837 cogeneration of reactive oxygen species for synergistic water treatment,  
838 Chemical Engineering Journal 358 (2019) 497–503.  
839 <https://doi.org/10.1016/j.cej.2018.09.192>.

840 [7] Y. Zhang, J. Zhan, B. Wang, J. Huang, S. Deng, G. Yu, S. Komarneni, Y. Wang,  
841 Integration of ultraviolet irradiation with electrochemical chlorine and hydrogen  
842 peroxide production for micropollutant abatement, Chemical Engineering Journal  
843 430 (2022) 132804. <https://doi.org/10.1016/j.cej.2021.132804>.

844 [8] P.J.M. Cordeiro-Junior, M.R. de V. Lanza, M.A. Rodrigo Rodrigo, Modeling the  
845 electrosynthesis of H<sub>2</sub>O<sub>2</sub>: Understanding the role of predatory species, Chem  
846 Eng Sci 273 (2023) 118647. <https://doi.org/10.1016/j.ces.2023.118647>.

847 [9] J. Li, Y. Li, Z. Xiong, G. Yao, B. Lai, The electrochemical advanced oxidation  
848 processes coupling of oxidants for organic pollutants degradation: A mini-  
849 review, Chinese Chemical Letters 30 (2019) 2139–2146.  
850 <https://doi.org/10.1016/j.cclet.2019.04.057>.

851 [10] I. Sánchez-Montes, G. O. S. Santos, T. O. Silva, R. Colombo, M. R. V. Lanza,  
852 An innovative approach to the application of electrochemical processes based on  
853 the in-situ generation of H<sub>2</sub>O<sub>2</sub> for water treatment, J Clean Prod 392 (2023)  
854 136242. <https://doi.org/10.1016/j.jclepro.2023.136242>.

855 [11] X. Liu, L. Chen, M. Yang, C. Tan, W. Chu, The occurrence, characteristics,  
856 transformation and control of aromatic disinfection by-products: A review, Water  
857 Res 184 (2020) 116076. <https://doi.org/10.1016/j.watres.2020.116076>.

858 [12] C. Li, G. Luo, Y. Liu, Comparison on the formation and toxicity for chlorinated  
859 products during the oxidation of acetic acid (CH<sub>3</sub>COOH) by three widely used  
860 advanced oxidation processes (AOPs) at the presence of Cl<sup>−</sup>, J Environ Chem  
861 Eng 11 (2023) 111501. <https://doi.org/10.1016/j.jece.2023.111501>.

862 [13] X. Xin, S. Sun, A. Zhou, M. Wang, Y. Song, Q. Zhao, R. Jia, Sulfadimethoxine  
863 photodegradation in UV-C/H<sub>2</sub>O<sub>2</sub> system: Reaction kinetics, degradation  
864 pathways, and toxicity, Journal of Water Process Engineering 36 (2020) 101293.  
865 <https://doi.org/10.1016/j.jwpe.2020.101293>.

866 [14] R.D. Acayaba, A.F. de Albuquerque, R.L. Ribessi, G. de A. Umbuzeiro, C.C.  
867 Montagner, Occurrence of pesticides in waters from the largest sugar cane  
868 plantation region in the world, Environmental Science and Pollution Research 28  
869 (2021) 9824–9835. <https://doi.org/10.1007/s11356-020-11428-1>.

870 [15] CÓDIGO MONOGRÁFICO NOME S13 S-METOLACLORO, n.d.

871 [16] I.J.S. Montes, B.F. Silva, J.M. Aquino, On the performance of a hybrid process to  
872 mineralize the herbicide tebuthiuron using a DSA® anode and UVC light: A  
873 mechanistic study, Appl Catal B 200 (2017) 237–245.  
874 <https://doi.org/10.1016/j.apcatb.2016.07.003>.

875 [17] G.F. Pereira, B.F. Silva, R. V Oliveira, D.A.C. Coledam, J.M. Aquino, R.C.  
876 Rocha-Filho, N. Bocchi, S.R. Biaggio, Comparative electrochemical degradation  
877 of the herbicide tebuthiuron using a flow cell with a boron-doped diamond anode  
878 and identifying degradation intermediates, *Electrochim Acta* 247 (2017) 860–  
879 870. <https://doi.org/10.1016/j.electacta.2017.07.054>.

880 [18] B.R. Gonçalves, A. Della-Flora, C. Sirtori, R.M.F. Sousa, M.C. V.M. Starling,  
881 J.A. Sánchez Pérez, E.M. Saggioro, S.F. Sales Junior, A.G. Trovó, Influence of  
882 water matrix components and peroxide sources on the transformation products  
883 and toxicity of tebuthiuron under UVC-based advanced oxidation processes,  
884 *Science of The Total Environment* 859 (2023) 160120.  
885 <https://doi.org/10.1016/j.scitotenv.2022.160120>.

886 [19] M.R.A. Silva, A.G. Trovó, R.F.P. Nogueira, Degradation of the herbicide  
887 tebuthiuron using solar photo-Fenton process and ferric citrate complex at  
888 circumneutral pH, *J Photochem Photobiol A Chem* 191 (2007) 187–192.  
889 <https://doi.org/10.1016/j.jphotochem.2007.04.022>.

890 [20] P.J.M. Cordeiro-Junior, J. Lobato Bajo, M.R. de V. Lanza, M.A. Rodrigo  
891 Rodrigo, Highly Efficient Electrochemical Production of Hydrogen Peroxide  
892 Using the GDE Technology, *Ind Eng Chem Res* 61 (2022) 10660–10669.  
893 <https://doi.org/10.1021/acs.iecr.2c01669>.

894 [21] R. da Silva Souto, L.P. de Souza, P.J.M. Cordeiro Junior, B. Ramos, A.C.S.C.  
895 Teixeira, R. da S. Rocha, M.R. V Lanza, Insights into Hydrodynamic and  
896 Operational Conditions for Scalable Hydrogen Peroxide Electrosynthesis  
897 Applications, *Ind Eng Chem Res* 62 (2023) 15084–15097.  
898 <https://doi.org/10.1021/acs.iecr.3c02139>.

899 [22] M.H. Silva, Use of computational toxicology (CompTox) tools to predict *in vivo*  
900 toxicity for risk assessment, *Regulatory Toxicology and Pharmacology* 116  
901 (2020) 104724. <https://doi.org/10.1016/j.yrtph.2020.104724>.

902 [23] W.R.P. Barros, T. Ereno, A.C. Tavares, M.R. V Lanza, In Situ Electrochemical  
903 Generation of Hydrogen Peroxide in Alkaline Aqueous Solution by using an  
904 Unmodified Gas Diffusion Electrode, *ChemElectroChem* 2 (2015) 714–719.  
905 <https://doi.org/10.1002/celc.201402426>.

906 [24] I.J.S. Montes, B.F. Silva, J.M. Aquino, On the performance of a hybrid process to  
907 mineralize the herbicide tebuthiuron using a DSA® anode and UVC light: A  
908 mechanistic study, *Appl Catal B* 200 (2017) 237–245.  
909 <https://doi.org/10.1016/j.apcatb.2016.07.003>.

910 [25] M.J. Watts, K.G. Linden, Chlorine photolysis and subsequent OH radical  
911 production during UV treatment of chlorinated water, *Water Res* 41 (2007)  
912 2871–2878. <https://doi.org/10.1016/j.watres.2007.03.032>.

913 [26] A.J.M. da Costa, M.S. Kronka, P.J.M. Cordeiro-Junior, G. V Fortunato, A.J. dos  
914 Santos, M.R. V Lanza, Treatment of Tebuthiuron in synthetic and real  
915 wastewater using electrochemical flow-by reactor, *Journal of Electroanalytical  
916 Chemistry* 882 (2021) 114978. <https://doi.org/10.1016/j.jelechem.2021.114978>.

917 [27] I. Sánchez-Montes, J.F. Pérez, C. Sáez, M.A. Rodrigo, P. Cañizares, J.M.  
918 Aquino, Assessing the performance of electrochemical oxidation using DSA®  
919 and BDD anodes in the presence of UVC light, *Chemosphere* 238 (2020)  
920 124575. <https://doi.org/10.1016/j.chemosphere.2019.124575>.

921 [28] X. Liu, M. Park, S.C. Beitel, C. Hoppe-Jones, X.-Z. Meng, S.A. Snyder,  
922 Formation of nitrogenous disinfection byproducts in MP UV-based water  
923 treatments of natural organic matters: The role of nitrate, *Water Res* 204 (2021)  
924 117583. <https://doi.org/10.1016/j.watres.2021.117583>.

925 [29] N. Kishimoto, State of the Art of UV/Chlorine Advanced Oxidation Processes:  
926 Their Mechanism, Byproducts Formation, Process Variation, and Applications, *J  
927 Water Environ Technol* 17 (2019) 302–335. <https://doi.org/10.2965/jwet.19-021>.

928 [30] J. Fang, Y. Fu, C. Shang, The Roles of Reactive Species in Micropollutant  
929 Degradation in the UV/Free Chlorine System, *Environ Sci Technol* 48 (2014)  
930 1859–1868. <https://doi.org/10.1021/es4036094>.

931 [31] M. Luna-Trujillo, R. Palma-Goyes, J. Vazquez-Arenas, A. Manzo-Robledo,  
932 Formation of active chlorine species involving the higher oxide MO<sub>x</sub>+1 on active  
933 Ti/RuO<sub>2</sub>-IrO<sub>2</sub> anodes: A DEMS analysis, *Journal of Electroanalytical Chemistry*  
934 878 (2020) 114661. <https://doi.org/10.1016/j.jelechem.2020.114661>.

935 [32] H. Yin, Q. Zhang, Y. Su, Y. Tang, M. Zhou, A novel UV based advanced  
936 oxidation process with electrochemical co-generation of chlorine and H<sub>2</sub>O<sub>2</sub> for  
937 carbamazepine abatement: Better performance, lower energy consumption and  
938 less DBPs formation, *Chemical Engineering Journal* 425 (2021) 131857.  
939 <https://doi.org/10.1016/j.cej.2021.131857>.

940 [33] F. Gozzi, I. Sirés, S.C. de Oliveira, A. Machulek, E. Brillas, Influence of  
941 chelation on the Fenton-based electrochemical degradation of herbicide  
942 tebuthiuron, *Chemosphere* 199 (2018) 709–717.  
943 <https://doi.org/10.1016/j.chemosphere.2018.02.060>.

944 [34] J.-F. Jen, M.-F. Leu, T.C. Yang, Determination of hydroxyl radicals in an  
945 advanced oxidation process with salicylic acid trapping and liquid  
946 chromatography, *J Chromatogr A* 796 (1998) 283–288.  
947 [https://doi.org/10.1016/S0021-9673\(97\)01019-4](https://doi.org/10.1016/S0021-9673(97)01019-4).

948 [35] I.F. Mena, M.A. Montiel, C. Sáez, M.A. Rodrigo, Improving performance of  
949 proton-exchange membrane (PEM) electro-ozonizers using 3D printing,  
950 *Chemical Engineering Journal* 464 (2023) 142688.  
951 <https://doi.org/10.1016/j.cej.2023.142688>.

952 [36] Á. Ramírez, M. Muñoz-Morales, F.J. Fernández-Morales, J. Llanos, Valorization  
953 of polluted biomass waste for manufacturing sustainable cathode materials for  
954 the production of hydrogen peroxide, *Electrochim Acta* 456 (2023) 142383.  
955 <https://doi.org/10.1016/j.electacta.2023.142383>.

956 [37] P. Pędziwiatr, F. Mikołajczyk, D. Zawadzki, K. Mikołajczyk, A. Bedka,  
957 Decomposition of hydrogen peroxide-kinetics and review of chosen catalysts,  
958 *Acta Innovations* (2018) 45–52. <https://doi.org/10.32933/ActaInnovations.26.5>.

959 [38] M.R.A. Silva, W. Vilegas, M.V.B. Zanoni, R.F. Pupo Nogueira, Photo-Fenton  
960 degradation of the herbicide tebuthiuron under solar irradiation: Iron  
961 complexation and initial intermediates, *Water Res* 44 (2010) 3745–3753.  
962 <https://doi.org/10.1016/j.watres.2010.04.025>.

963 [39] G.F. Pereira, B.F. Silva, R. V Oliveira, D.A.C. Coledam, J.M. Aquino, R.C.  
964 Rocha-Filho, N. Bocchi, S.R. Biaggio, Comparative electrochemical degradation  
965 of the herbicide tebuthiuron using a flow cell with a boron-doped diamond anode  
966 and identifying degradation intermediates, *Electrochim Acta* 247 (2017) 860–  
967 870. <https://doi.org/10.1016/j.electacta.2017.07.054>.

968 [40] S. Kali, M. Khan, M.S. Ghaffar, S. Rasheed, A. Waseem, M.M. Iqbal, M. Bilal  
969 khan Niazi, M.I. Zafar, Occurrence, influencing factors, toxicity, regulations, and  
970 abatement approaches for disinfection by-products in chlorinated drinking water:  
971 A comprehensive review, *Environmental Pollution* 281 (2021) 116950.  
972 <https://doi.org/10.1016/j.envpol.2021.116950>.

973 [41] United Nations, Globally Harmonized System of Classification and Labelling of  
974 Chemicals (GHS), Geneva, 2023. <https://unece.org/sites/default/files/2023-07/GHS%20Rev10e.pdf> (accessed April 15, 2024).

976 [42] I. Sánchez-Montes, G.O.S. Santos, A.J. dos Santos, C.H.M. Fernandes, R.S.  
977 Souto, P. Chelme-Ayala, M.G. El-Din, M.R. V Lanza, Toxicological aspect of  
978 water treated by chlorine-based advanced oxidation processes: A review, *Science of The Total Environment* 878 (2023) 163047.  
980 <https://doi.org/10.1016/j.scitotenv.2023.163047>.

981 [43] H.L. Barazorda-Ccahuana, A.S. Fajardo, A.J. dos Santos, M.R. V Lanza,  
982 Decentralized approach toward organic pollutants removal using UV radiation in  
983 combination with H<sub>2</sub>O<sub>2</sub>-based electrochemical water technologies, *Chemosphere*  
984 342 (2023) 140079. <https://doi.org/10.1016/j.chemosphere.2023.140079>.

985 [44] H. Feng, X. Liao, R. Yang, S. Chen, Z. Zhang, J. Tong, J. Liu, X. Wang,  
986 Generation, toxicity, and reduction of chlorinated byproducts: Overcome  
987 bottlenecks of electrochemical advanced oxidation technology to treat high  
988 chloride wastewater, *Water Res* 230 (2023) 119531.  
989 <https://doi.org/10.1016/j.watres.2022.119531>.

990 [45] Z. Tasic, V.K. Gupta, M.M. Antonijevic, The Mechanism and Kinetics of  
991 Degradation of Phenolics in Wastewaters Using Electrochemical Oxidation, *Int J  
992 Electrochem Sci* 9 (2014) 3473–3490. [https://doi.org/10.1016/S1452-3981\(23\)08025-2](https://doi.org/10.1016/S1452-3981(23)08025-2).

994 [46] O. Gomes Júnior, M.G.B. Santos, A.B.S. Nossol, M.C.V.M. Starling, A.G.  
995 Trovó, Decontamination and toxicity removal of an industrial effluent containing  
996 pesticides via multistage treatment: Coagulation-flocculation-settling and photo-

997 Fenton process, Process Safety and Environmental Protection 147 (2021) 674–  
998 683. <https://doi.org/10.1016/j.psep.2020.12.021>.

999

1000

1001